Batteries & Supercaps

Research Article
doi.org/10.1002/batt.202500126

Chemistry Europe
European Chemical Societies Publishing

www.batteries-supercaps.org

Stress-Induced Failure Analysis of High-Capacity SiO_x/Graphite Composite Anodes

Hebin Zhang, Junpo Guo,* Bing Han, Yun Zheng, Yingying Shen, Yike Huang, Yinan Liu, Zenan Li, Qi Zhang, Wei Jiang, Yunxian Qian, Pengli Zhu, Jun Wang,* and Huaiyu Shao*

The structural evolution of silicon oxide/graphite (SiO_x/Gr) composite anodes under SiO_x expansion is systematically investigated to address the lack of in-depth studies on the mechanical disparities between Si-based materials and graphite during operation. In this work, the electrode structure evolution is evaluated with a series of composite anodes with different SiO_x/Gr ratios through electrochemical performance tests and structural characterization, focusing on pore growth and solid electrolyte interphase (SEI) renewal induced by active material volume changes. The results reveal that the continuous volume change of SiO_x leads to uneven stress distribution within the electrode, which further causes mechanical fatigue and structural fractures of active materials. Notably, the replacement of modified SiO_x material with artificial coating improves structural integrity and cycling performance, enabling the composite anode to maintain a capacity of 373 mA h g^{-1} even at 1 A g^{-1} after 1000 cycles. These findings demonstrate that optimizing stress distribution and structural evolution is critical for enhancing the mechanical stability and electrochemical performance of SiO_x/Gr composite anodes. This study provides fundamental insights into the failure mechanisms of SiO_x/Gr composite anodes and highlights the necessity of rational electrode design strategies to develop high-capacity, long-cycle-life anode materials for next-generation lithium-ion batteries.

1. Introduction

Lithium-ion batteries (LIBs) are now a common feature in a wide range of applications, extending beyond portable electronics and electric vehicles. This growing use has led to an increased demand for rechargeable batteries with higher energy density and better cycling performance. Given that the conventional graphite anode only provides a stable capacity of about 372 mA h g^{-1} for LiC_6,[1] Si-based material has drawn considerable interest from numerous researchers due to its abundance on earth and high theoretical capacity.[2] However, in contrast to the intercalation mechanism of graphite,[3] Si-based material exhibits poorer conductivity and is subject to significant volume expansion (≈300% for pure Si) during the alloying and dealloying reactions.[4] This inevitable volume expansion could produce large stress on the interface of active material and disrupt the conducive pathways,[5] resulting in structural damage, irreversible depletion of lithium-ion, and other side reactions, which finally lead to capacity loss.[6] Silicon suboxide (SiO_x, $0 < x \leq 2$) represents a promising alternative to pure Si, exhibiting a smaller volume expansion (≈160%) while maintaining a relatively high capacity of ≈2000 mA h g^{-1}.[7] Accordingly, the co-utilization of Si-based material and carbonaceous material has become a preferred strategy aimed at improving energy density and cycling stability.[8] Particle sizes and crystallographic structures of carbons were varied to create precursors for combining with Si-based materials, among which SiO_x/Gr composites have attracted particular interest due to their compatibility with established battery

H. Zhang, Y. Zheng, Y. Shen, Y. Huang, Y. Liu, Q. Zhang, W. Jiang, H. Shao
Institute of Applied Physics and Materials Engineering
University of Macau
Macao SAR 999078, China
E-mail: hshao@um.edu.mo

H. Zhang, P. Zhu
Shenzhen Institute of Advanced Electronic Materials
Shenzhen Institute of Advanced Technology
Chinese Academy of Sciences
Shenzhen 518055, China

J. Guo
Collaborative Innovation Center of Henan Province for Green Manufacturing of Fine Chemicals
Key Laboratory of Green Chemical Media and Reactions
School of Chemistry and Chemical Engineering
Henan Normal University
Xinxiang 453007, China
E-mail: guojunpo@htu.edu.cn

B. Han
Eastern Institute for Advanced Study
Eastern Institute of Technology
Ningbo 315200, China

Z. Li, J. Wang
Department of Materials Science and Engineering
School of Innovation and Entrepreneurship
Southern University of Science and Technology
Shenzhen 518055, China
E-mail: wangj9@sustech.edu.cn

Y. Qian
Shenzhen CAPCHEM Technology Co., Ltd.
Shenzhen 518118, China

Supporting information for this article is available on the WWW under https://doi.org/10.1002/batt.202500126

manufacturing processes.[9] However, the volume change is still widely recognized as the dominant reason for the rapid capacity loss, poor cycling performance and low Coulombic efficiency (CE) of SiO_x materials.[10]

Various attempts have been conducted to explore the capacity fading mechanism and resolve the challenge of Si-based/graphite composite anode. Wu et al. explain the incompatibility between Si-based and graphite materials in their composite anode during operation, and the obvious volume change and repetitive solid electrolyte interphase (SEI) recombination of Si-based particles tend to reduce their connection with graphite, thus resulting in poor cycling performance.[11] Currently, it is widely attributed to the composite anode failure to the expansion of Si-based materials, which induces the cumulative mismatch stress distribution.[12] Moon et al. established a unique structure–activity relationship between capacity decay and the stress evolution of Si-based/graphite anode through Li^+ crosstalk analysis. It is also indicated that the cumulative mismatch stress arising from the obvious volume change of Si material tends to inhibit Li^+ intercalation into graphite structure, thereby reducing the capacity of the composite anode. Enhancing the cycling performance can be achieved by reducing the particle size of the Si and increasing the hardness of the graphite, which facilitates the homogeneity of the electrochemical reactions in both the Si and graphite.[13] Dose et al. demonstrated that the mechanical stress evolution would damage both Si and graphite material structure, thus leading to SEI breakdown/reorganization, Li^+/e^- channel interruption, and polarization increment. As a result, the as-prepared Si–graphite anode delivered a relatively low capacity retention of 75% at its 100th cycle.[14]

Further research has attempted to understand the interactions that occur between Si-based materials and graphite in the composite electrode. Lee et al. investigated the thermal impact on the SiO/graphite composite anode and demonstrated that SiO accelerates the de-intercalation of graphite, which results in a preferential side reaction toward SiO and the loss of lithium inventory. It was discovered that the SiO/graphite composite with a high-temperature storage process would have a high recovery capacity of 2.6 mA h cm^{-2} after 8 weeks. This demonstrates the positive role of thermal treatment on stress release, thus maintaining material structural integrity and extending its cycling life.[15] Furthermore, the lithium-ion storage behavior of SiO_x/C composite anodes has been established as being dependent on the carbon microstructure. A carbon microstructure with greater disorder may result in higher capacitive contribution from graphite and reduced superficial compressive stress on SiO_x, thereby enhancing the electrochemical properties, such as the delivered high-capacity retention of 78% after 100 cycles observed in SiO_x/soft carbon anodes. Nevertheless, the increased specific surface area and greater abundance of defect sites in carbon will consume a greater quantity of active lithium, which restricts its deployment in full cells.[16] Such constraints have previously been identified as disturbing the lithium-ion kinetics and are related to capacity fading. This in turn has resulted in the low addition of silicon-based materials in composite anodes, thereby further limiting their application in fast-charging. However, based on the previous reports, the capacity degradation of SiO_x/C composite electrodes is mainly analyzed from the material level, and the effect of the overall structural damage of the electrode has not been subjected to systematic investigation. This oversight is a crucial aspect that is the main macroscopic and direct cause of battery failure and must be addressed to enhance the reliability and longevity of batteries.

To better comprehend how the SiO_x expansion-induced alterations to graphite exert a significant influence and the precise mechanism of the capacity decay as observed in the SiO_x/Gr composite anodes, it is essential to consider the internal stress distribution and the structural integrity of the electrodes. In this work, insights are presented in a detailed account of the corresponding structural changes and electrochemical performance of the SiO_x/Gr electrodes. These composite anodes possess theoretical capacities of 600 mA h g^{-1} (SiOGr-600), 800 mA h g^{-1} (SiOGr-800), and 1000 mA h g^{-1} (SiOGr-1000), and are manufactured by adjusting the amount of active material (Table S1, Supporting Information). It is demonstrated that the expansion-shrinkage process of the SiO_x material has the potential to increase the internal stress concentration, leading to permanent changes in the electrode in terms of electrode cracking and SEI regeneration. Overtime, the thickened SEI performs increasing polarization and larger overpotential after long-term cycling, which hinders the lithium-ion transfer and thus facilitates capacity loss. Furthermore, by substituting the conventional SiO_x material, the structural stability of the composite anodes shows great improvement because the artificial coating on the modified SiO_x can effectively mitigate against the stress accumulated during the service period. This work offers a novel perspective on the capacity decay mechanism analysis and a potential solution for high-capacity SiO_x/Gr composite anode, which is beneficial to improve the energy density and lifetime of Si-based batteries, thereby enhancing their application scenarios in the future.

2. Results and Discussion

2.1. Electrode Structural Failure

The characterization of graphite and SiO_x anode materials is presented in **Figure 1**a and S1, Supporting Information. Compared with amorphous pure SiO_x, the commercial SiO_x exhibits several weak crystalline phases, which are indicative of the carbon coating by chemical vapor deposition and carbonization. The valence state of SiO_x is presented in Figure S2, S3 and Table S2, S3, Supporting Information. The materials were then mixed in specific ratios to prepare electrodes with different capacities as shown in Figure S4, Supporting Information. The composite electrodes exhibit characteristic peaks corresponding to SiO_x and the (002) peak of graphite, along with a set of peaks from the copper foil. These results further verify the composition of anode material and confirm the crystallinity of each component. As the SiO_x content increases, the elastic modulus and stiffness of the material also change (Figure 1b,c). The addition of SiO_x results in a higher stiffness and larger modulus, which makes the material less vulnerable to external stress and reduces the likelihood of yielding. Although graphite is less rigid than SiO_x during the deformation

Research Article
doi.org/10.1002/batt.202500126
Chemistry Europe
European Chemical Societies Publishing

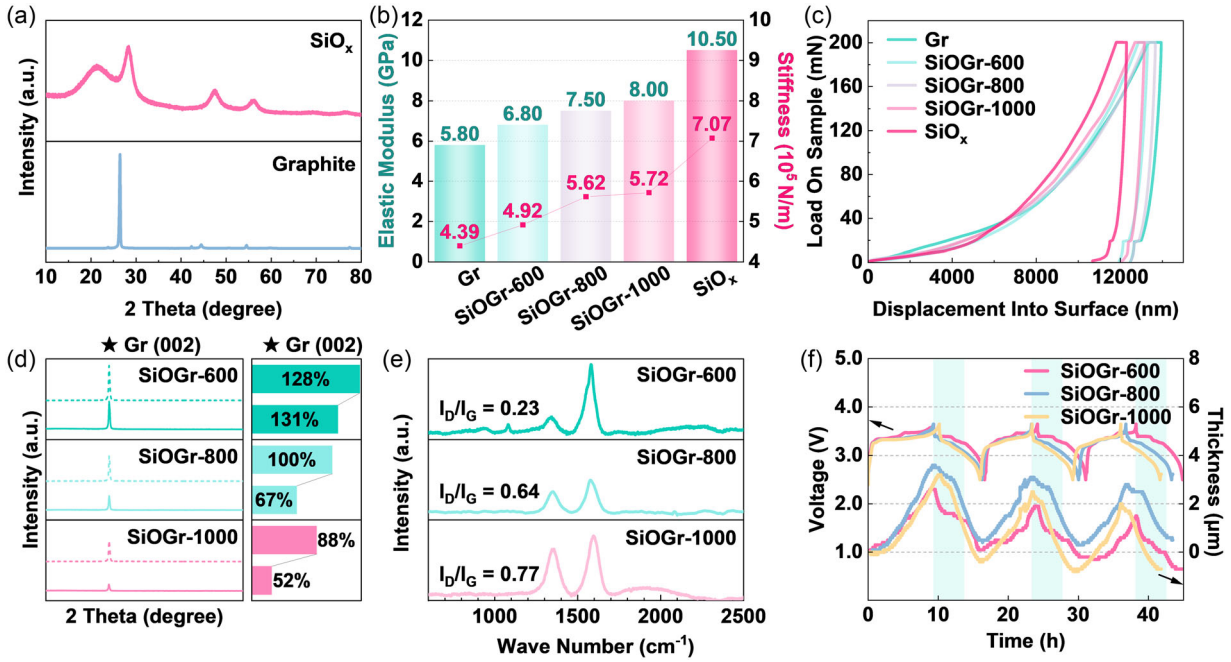

Figure 1. a) XRD pattern of pristine SiO_x and graphite anode materials. b) Elastic modulus and stiffness comparison of different electrode materials. c) Stress–strain curves attained from nano-indentation test. d) XRD patterns before (dotted line) and after (straight line) 5 cycles at 0.05C and normalized crystal intensity of graphite in composite anodes with different capacities. e) Raman spectra of electrodes after 5 cycles. f) Coin-cell thickness change (bottom) and voltage change (top) of full cells in the first 3 cycles.

stage, it also displays a relatively low elastic modulus, which limits its ability to recover from deformation. Consequently, the material provides less buffering to outer compression, increasing the probability of permanent damage to the structure.

This brittle property could be reflected in the loss of crystallinity after only a few cycles (Table S4, Supporting Information). Initial Coulombic efficiency (ICE) was first determined for the well-prepared electrodes. As demonstrated in Figure S5 and S6, Supporting Information, all three groups of fully activated electrodes exhibit a stable ICE of ≈76%, which is relevant to the cost of lithium ions in forming SEI, and the ICE gradually decreases with the addition of SiO_x. However, it was observed that the CE could be enhanced to ≈99% after five cycles, at which point the side reaction of lithium ions is significantly reduced due to the stability of the SEI. Consequently, the electrodes attain the capacity to fully discharge and recharge in each cycle. Figure 1d shows the X-ray diffraction (XRD) pattern after 5 cycles, demonstrating a severe decline in the crystallinity of graphite compared to SiOGr-600, SiOGr-800, and SiOGr-1000. All data have been normalized with the intensity of the copper foil to reduce the intergroup error. The notable crystallinity loss reaches 36% in SiOGr-1000 compared to the initial pristine electrodes. In addition, the Raman spectra in Figure 1e provide evidence of damage to the graphite microstructure. The value of I_D/I_G which indicates the graphitization degree has decreased from 0.77 to 0.23 when the SiO_x content increases from 16.7 (SiOGr-600) to 44.4% (SiOGr-1000). This gradual loss of order degree and rising carbon defect are associated with the increasing SiO_x content in the composite electrode. The disruption of the long-term order parameter of graphite caused by the expansion of SiO_x particles leads to a reduction in the degree of graphitization.

In addition, the overall structure of the electrode also has a macroscopic expansion, and the monitoring of electrode thickness in Figure 1f shows a discrepancy following the SiO_x content. During the discharging process, the stage above 3.22 V refers to the working potential of graphite, at which the thickness recovers from the last charging swelling.[14] In both the SiOGr-600 and SiOGr-1000 groups, a relatively symmetrical swelling and retraction peak is observed, which is correlated with the mild SEI accumulation and acceptable total expansion of the electrode.[17] However, an obvious discriminative slope is evident for the SiOGr-800 group, whereby it is unable to fully retract due to the repeating SEI generation, demonstrating the largest thickening effect of the graphite component. As exhibited in Figure 1f, the net expansion of the electrodes reaches its maximum value in this group, while the expansion of the electrodes per unit capacity increases in proportion to the SiO_x content (Table S5 and S6, Supporting Information).

2.2. SEI Accumulation and Resulted Insufficient Lithiation

The ongoing structural damage and particle fragmentation would expose the fresh graphite surfaces and initiate a new SEI growth process, which should only occur during the first few lithiation processes.[18] The conventional depiction of the SEI comprises insoluble reduction products of electrolyte constituents, including lithium salts and solvents.[19] The working potential is the primary factor determining the electrolyte decomposition products and the structural evolution of the SEI.[18] Consequently, each anode material will exhibit a specific distribution of organics and inorganics at a defined electrode

Research Article
doi.org/10.1002/batt.202500126
Chemistry Europe
European Chemical Societies Publishing

potential.[20] In the case of a graphite anode, the bilayer structure is observed at low potential (0 V), while the mosaic structure is only evident at high potential (3 V).[21] Therefore, for a fully delithiated graphite anode, the distribution of organics and inorganics should be more uniform throughout the subsurface and surface of the SEI. To provide a more detailed illustration of this trend, depth-profiling X-ray photoelectron spectroscopy (XPS) was employed to detect the SEI composition at greater depths,[22] comprising a series of elements as illustrated in **Figure 2**a,b. The fully charged electrodes after 5 cycles were selected as a reference to eliminate the potential interference of intercalation compounds and alloys.

After cycles, the total composition of the SEI throughout electrodes from surface to subsurface was sufficient to distinguish the groups, as illustrated in Figure 2c,d. In the case of the pure graphite anode, the SEI displays a slightly lower ratio of organics in the outer layer and a lower ratio of inorganics in the inner layer in comparison with the SiO_x anode. This results in a slight and gentle decrease trend of organics in the SEI of graphite, while that in the SEI of SiO_x exhibits the opposite, presenting a rapid decay of organics. In the SiOGr-600, the graphite microstructure is preserved intact due to the low content of SiO_x material and less damage caused by its expansion. At this time, the SEI on the composite anode mainly exhibits characteristics similar to that on the SiO_x, and the obvious bilayer feature can still be distinguished. However, when the mass ratio of SiO_x increases from 16.7% (SiOGr-600) to 30.6% (SiOGr-800), a decrease of organics in the outer layer is observed, accompanied by an increase in the inner layer organics. The SEI on SiOGr-800 exhibits a gentler overall trend of organics that is more similar to that on pure graphite, even with lower graphite content, rather than exhibiting an according transformation with the increasing SiO_x. It is then inferred that SiOGr-600 receives less compression from fewer SiO_x particles, thus less SEI on graphite exists in the anode electrode. But for the SiOGr-800 which experiences more severe compression from SiO_x, the uneven stress distribution first exerts SEI growth on the graphite surface. In this composite anode with the dominant content of graphite, more SEI on graphite means the overall trend of SEI composition will exhibit a peculiarity that is more like observed in the pure graphite anode. Furthermore, as the mass ratio of SiO_x reaches 44.4% (SiOGr-1000), there is a notable change in the composition due to the dominance of the SEI on SiO_x, which is generated by the increasing SiO_x content. The negative effects on graphite SEI caused by the compression from SiO_x are counteracted by the reduction in graphite content. This is further manifested as an expanded fluctuation range of the organic/inorganic ratio from the outer layer to the inner layer, which resembles that of the SEI on a pure SiO_x anode. This phenomenon observed in XPS also shows consistency with the thickness change monitoring of electrode results.

This abnormal trend in SEI transformation also correlates with lithium-ion storage and release. The activated SiO_x anode has a working potential of 0–1 V versus Li/Li^+, which is higher and more precipitous than Si, whereas the graphite anode typically operates at a potential of below 0.2 V.[23] This discrepancy in working potential precludes the simultaneous lithiation/delithiation of these two materials in the composite anode, necessitating instead a sequential process. The SiO_x anode is invariably the first to undergo lithiation, whereas the graphite anode is intercalated first in the process of delithiation. The inhomogeneous nature of the composite anode could also result in predictable severe polarization of a single component.[24] The lithiation/delithiation

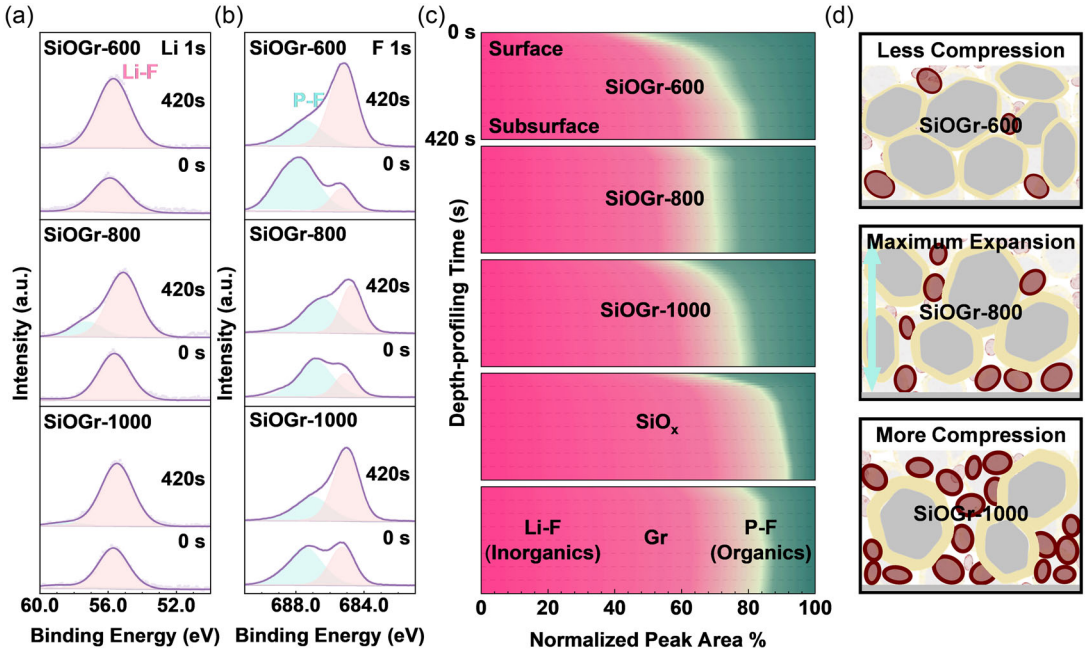

Figure 2. a–c) XPS depth-profiling spectra of composite anodes after 5 cycles at 0.05C: a) Li 1s, b) F 1s, and c) statistical results of Li–F and P–F content. The normalized peak area (colormap) has been corrected by sensitive factors. Li–F from Li 1s (pink) and P–F from F 1s (green) are specifically chosen to represent the inorganic and organic ratios in SEI, respectively. d) Schematic figure of the relationship between SEI growth and electrode thickness of composite anodes after cycling. Graphite is shown as grey particles with the SEI being shown as a yellow layer, and the SiO_x is shown as red particles.

Research Article
doi.org/10.1002/batt.202500126
Chemistry Europe
European Chemical Societies Publishing

state calculated from GCD profiles (Figure S7 and S8, Supporting Information) shows the capacity contribution of each anode component, where the second stage of delithiation and the first stage of lithiation correspond to the reactions on the SiO_x anode. It can be observed that even after 500 cycles, the SiO_x component exhibits a greater charging capacity contribution, whereas the graphite component demonstrates a comparable discharging capacity contribution. Given that the lithium ions have a higher diffusion coefficient during the deintercalation than during the intercalation,[1] this variation in the contribution is most likely attributable to the interfacial deactivation caused by the layered SEI. It is also indicated that due to the discrepancy in SiO_x content, the actual capacity may not only be evaluated and decided by the SEI composition. Therefore, the detailed electrochemical performance is investigated by d*Q*/d*V* profiles and constant voltage (CV) curves in **Figure 3**. According to the working potential, a sequential lithiation is exhibited, which would result in the interfacial ion transfer from SiO_x to graphite in lithium-ion intercalation.

During the lithiation stage, the results demonstrate an overall deferred sequential lithiation after 500 cycles, as illustrated in Figure 3a–d. This phenomenon can be attributed to the regenerating layered SEI on graphite, which impedes the lithium-ion transfer from both the electrolyte and the SiO_x particles. For SiOGr-600 in Figure 3b, all reduction peaks shift to a lower potential, yet remain fully in three stages. This corresponds to the larger resistance for lithium ions intercalation and later graphite intercalation compounds (GIC) formation in each step. During the delithiation stage, the initial two oxidation peaks, occurring at ≈0.15 V, exhibit a reduction in magnitude, contributing less to the overall discharging capacity. Conversely, the final oxidation peak, occurring at 0.22 V, corresponds to the phase evolution from LiC_6 to LiC_{12} and demonstrates a delay, suggesting that the delithiation process for graphite may be insufficient. In the group with a higher SiO_x content (SiOGr-800) in Figure 3c, while the delay is consistent with that observed in the former group, the reduction peaks all begin to shrink due to an evident capacity loss after 500 cycles. It is evident that the capacitive contribution is directly proportional to the degree of disorder in the carbon component of SiO_x/C composite anodes. This implies that disordered carbon is more effective in contributing to capacity due to its ability to accommodate a wider and similar working potential.[24] However, this increase in capacity contribution in the composite anode is offset by the decrease in graphite content, resulting in a gradual decline in reversible capacity during extended cycling. Moreover, the rearranged graphite should exhibit a larger specific surface area and a relatively broad lithiation potential. The enlarged surface area promotes the total diffusion kinetics of lithium ions, and the alteration in working potential facilitates enhanced compatibility with that of SiO_x, thereby partially merging the peaks from the sequential lithiation process.

Given the considerable damage to the graphite in the SiOGr-1000, the sharp lithiation peaks collapse into a broad slope-like curve comprising two stages as shown in Figure 3d. The stable wide peak centered around 0.15 V (stage 1) is attributed to the simultaneous formation of SiO_x alloying and intermediate GICs (LiC_x); the remaining part is ascribed to short-range ordered graphite resulting from inadequate lithiation (stage 2), during which the intermediate GICs with lower atomic ratios of lithium (LiC_y, $y > 12$) are generated. A similar situation can be observed in the remaining two oxidation peaks, and the only one pertaining to graphite occurs at ≈0.22 V. The capacity loss indicated by the peak damping should be attributed to the insufficient lithiation of graphite during the previous charging process, rather than attributed to the sluggish lithium-ion diffusion because the deintercalation process has a higher diffusion coefficient. This suggests that intermediate GICs are formed with lower atomic ratios of

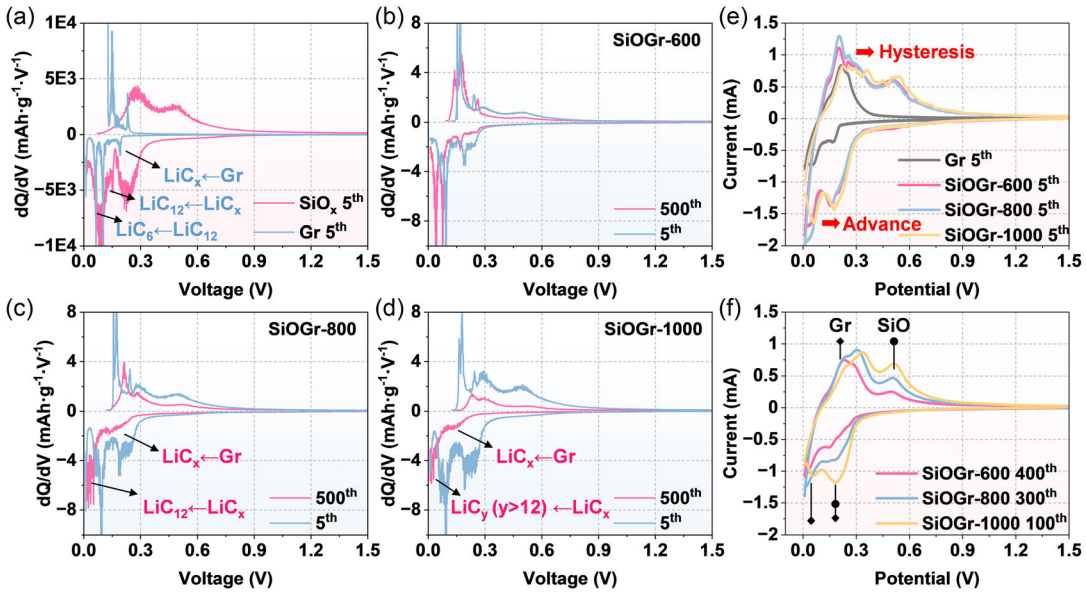

Figure 3. a–d) Galvanostatic d*Q*/d*V* curves of a) pure graphite and SiO_x in the 5th cycle, and b) SiOGr-600, c) SiOGr-800, and d) SiOGr-1000 in the 5th and 500th cycle at 0.5 A g^{-1}. e,f) CV curves of e) the 5th cycle and after f) midterm cycling.

lithium and that a complete lithiation stage with a perfect composition of LiC_6 cannot be achieved in the presence of active material loss.

CV curves presented in Figure 3e,f provide a detailed account of the charge/discharge behavior observed in the 5th cycle and after subsequent specified intermediate cycling. In this subsequent cycle, the composite anodes show comparable capacity retention rates (Figure S9, Supporting Information). This is undertaken to evaluate the electrochemical behavior under incipient damage and moderate damage. It is easy to notice that the oxidation process exhibits two isolated peaks, which correspond to graphite (≈0.2 V) and SiO_x (≈0.5 V), respectively, when compared with the CV curve of graphite in Figure 3e. Conversely, during the reduction process, the first peak of graphite (≈0.15 V) is particularly prominent, thereby masking the broader reduction peak of SiO_x. As presented in Figure 3f, the oxidation peak of SiO_x persists after midterm cycling in all three composites, and the current intensity is even greater for the composite with a higher SiO_x content. It appears that the alloying of SiO_x is effectively preserved in the group even with a higher SiO_x content, which serves to demonstrate the capability of SiO_x capacity retention. In contrast, the oxidation peaks for graphite exhibit a hysteresis, as illustrated in the dQ/dV profile in the 500th cycle. Ultimately, the main oxidation peak of graphite shifts to a higher potential, caused by pairing with the electron transfer with SiO_x and the incomplete lithiation of graphite, leading to delayed delithiation in the charging process.

The reduction peak at higher potential (≈0.15 V) shows a comparable result to the oxidation process of SiO_x, whereas the second reduction peak for graphite (<0.1 V) displays a distinct behavior as presented in Figure 3f. The increased peak value for SiOGr-800, which corresponds to the later period lithiation of graphite, indicates greater ion kinetics, which may be led by the direct phase transfer from SiO_x to graphite. This also signifies that by this point, the accumulated SEI has not impeded the reaction rate, allowing the lithium ions to transfer from both electrolyte and SiO_x through SEI. However, for SiOGr-1000 in the 100th cycle, the current density on the graphite is evidently reduced and for the first time lower than that at higher potential. This is ascribed to the accumulated structure failure of graphite decelerating the reduction rate. In this instance, the reduction peak center also shifts to a higher potential, approaching that of the SiO_x and earlier graphite reduction. The observed advanced reduction indicates that with an increased SiO_x content, direct phase transfer would be the dominant mechanism, which makes it also susceptible to inward compressive stress from bidirectional diffusion.[24] Consequently, the irreversible structural damage affects the final stage of the electrochemical reaction, leading to the irreversible capacity loss of graphite.

2.3. Electrode Crack Growing

The examination of the anode electrode after post-cycling reveals a cracking phenomenon that has rarely been reported before, which verifies the failure mechanism described in the previous section. **Figure 4**a shows the particle size distribution and average size of two anode materials. It can be observed that the pristine graphite particle has a larger pellet, which is approximately four times the size of the SiO_x material. However, when the graphite is composited with SiO_x in the composite anode, the composite electrodes exhibit facial cracking only after 5 cycles. This phenomenon is not observed in pure graphite anode material, as evidenced by the scanning electron microscope (SEM) image of the electrode surface shown in Figure 4b1 and b2. In addition, the clear crack pattern of electrodes can be observed in the composite anode after cycling. The interlayer exfoliation of graphite or bonding failure described in Figure 4e is contingent upon the shape of the materials and the distribution of the material. As an example, SiO_x particles distributed alongside the graphite layers could expand the interlayer distance of graphite, leading to exfoliation and the potential formation of a continuous crack (Figure 4c). This phenomenon may occur due to the overcoming of the van der Waals force, which could otherwise act to maintain the integrity of the layers. In the event of multiple SiO_x particles initially situated between graphite layers, repeated expansion would have a disruptive effect on the adhesion (Figure 4d), ultimately leading to the bonding failure and the separation of the surfaces, creating a gap for the next round of SEI deposition. Both types of cracks have reserved space for the electrolyte, and an SEI would be deposited on the newly exposed surface of the anode material.

Additionally, it has been observed that the width of the crack resulting from interlayer exfoliation is typically shorter and more coherent than that caused by other mechanisms as shown in Figure 4f. This phenomenon can be attributed to that the van der Waals force provides a stronger cohesion force than that of a typical chemical adhesion agent. With regard to bonding failure, the amount of SiO_x particles appears to be a significant factor. When the crack is controlled by two corresponding SiO_x particles on either side, the resulting gap is wider. SEM images reveal that apart from the expansion and damage of the SiO_x material, the increased cracking and growing pores of the electrode are also serious causes of capacity fading and electrode failure.

To demonstrate the composite anode capability, rate performances at various current densities are conducted to verify a reliable SiO_x/Gr proportion of practical importance (**Figure 5**a and S9, Supporting Information). For a traditional SiO_x/Gr anode, an economically viable option may be to utilize a minor SiO_x content of less than 20%. It has been observed that an increase in SiO_x addition beyond this threshold does not result in a notable enhancement in capacity, even after multiple cycles of rate charging/discharging. All three groups reach a relevant stable capacity of around 550 mA h g^{-1} while the SiOGr-800 could maintain a slightly larger capacity of 570 mA h g^{-1} in the reported experiment. This outcome is likely to benefit from the formation of a firm and proper SEI. Further, the addition of a higher amount of SiO_x may potentially compromise the long-term cycling performance at high current densities.

Replacement of SiO_x material is another route to improve the overall performance of composite anodes with higher SiO_x addition. The associated findings are presented in Figure 5b–f. The a-SiO_x is a commercialized modified SiO_x material with an artificial carbon-based protective layer. As shown in Figure S10–S12,

Research Article
doi.org/10.1002/batt.202500126
Chemistry Europe
European Chemical Societies Publishing

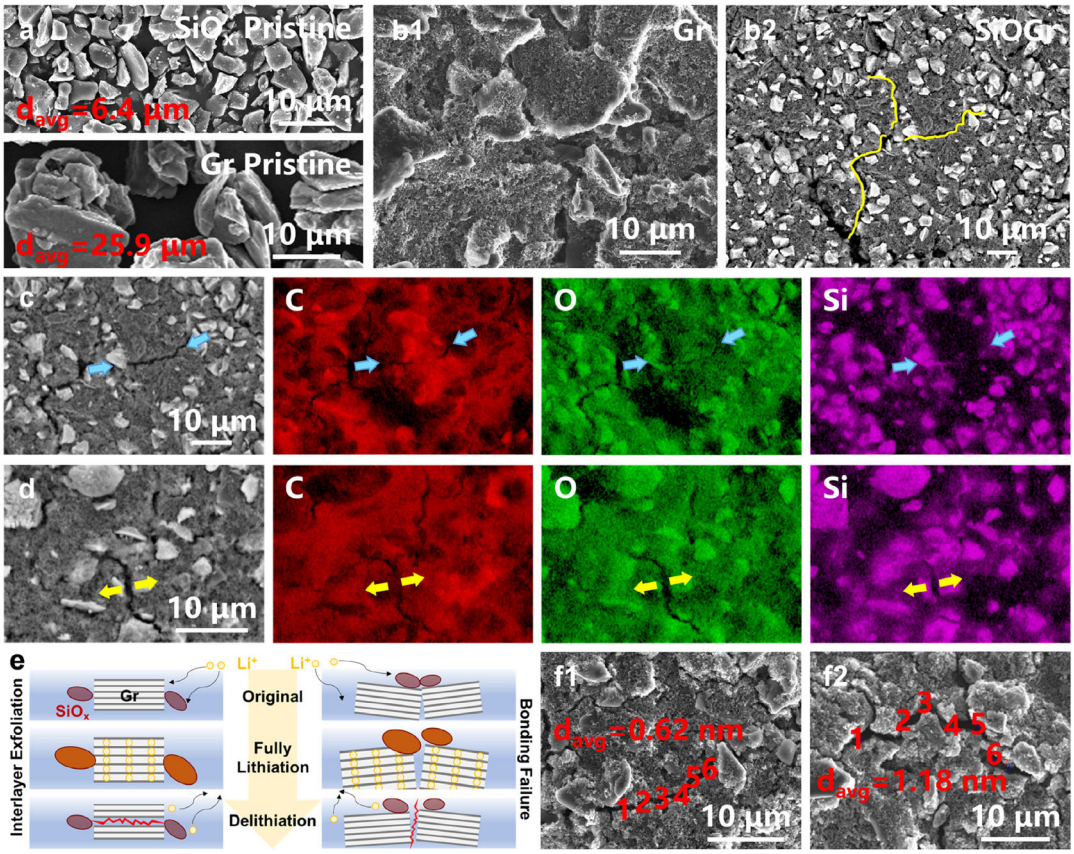

Figure 4. a) Morphology and particle size of pristine SiO_x and graphite material. b) The electrode surface of graphite anode and composite anode after 5 cycles at 0.05C. c,d) SEM and energy-dispersive X-ray spectroscopy (EDS) images of two patterns of crack: c) interlayer exfoliation and d) bonding failure. e) Schematic figure of particle deformation in two crack patterns. f) Crack width statistics in f1) the interlayer exfoliation and f2) bonding failure pattern.

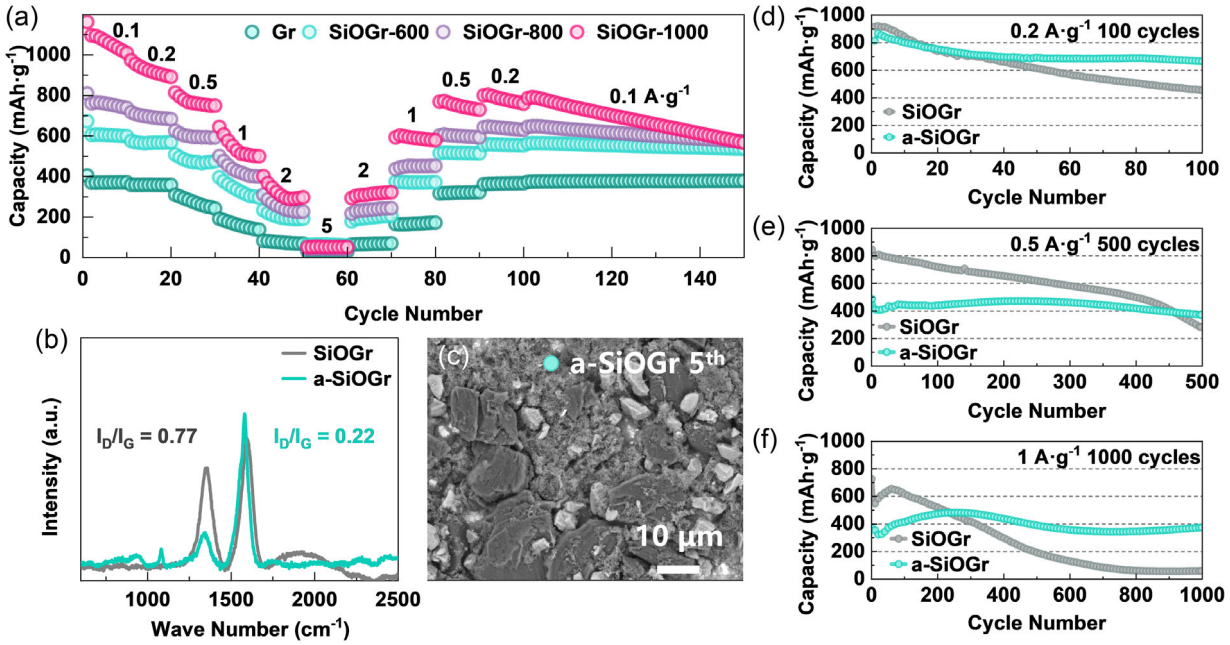

Figure 5. a) Rate performance of composite anodes with different capacities. b) Raman spectra of SiOGr and a-SiOGr electrodes. c) SEM image of electrode surface of a-SiOGr after 5 cycles. d–f) Capacity retention rate comparison at different current densities: d) 0.2 A g^{-1}, e) 0.5 A g^{-1}, and f) 1 A g^{-1}.

Supporting Information, the a-SiO_x contains an amorphous coating layer that exhibits strengthened C—O and C═O signals, which offers an additional buffer to low-current-density cycling and relieves the structural damage. Upon replacing the SiO_x into a-SiO_x, the composite anode with 44.4% a-SiO_x exhibited a capacity of 373 mA h g^{-1} even at 1 A g^{-1} after 1000 cycles, whereas the SiOGr nearly lost all its capacity (Figure 5f). In addition, Raman spectra (Figure 5b) and SEM images (Figure 5c) are employed to examine the microstructure of graphite materials and the morphology of electrodes prepared via the same procedure. It appears that the proper modification of SiO_x could effectively protect the electrode from cracking and even maintain the long-range ordered structure. The well-designed coating layer may facilitate an accelerated rate of interface reaction, subsequently enabling the a-SiOGr composite anodes to achieve equilibrium CE at a more rapid rate than raw SiO_x material composited with graphite.

3. Conclusion

In summary, the SiO_x material with the high expansion coefficient disturbs the stress distribution within the SiO_x/Gr composite electrode during charge/discharge cycles, which results in a series of structural failures due to the discrepancy in mechanical properties. This study examined the structural evolution pattern and related signals to ascertain the interaction between the two types of materials in SiO_x/Gr composite anodes with varying capacities. Initially, graphite acquires short-range crystalline defects during the first few cycles, and the uneven stress distribution causes a decrease in the degree of order. Concurrently, the electrode suffers from deformation and pore growth due to undissipated internal stresses caused by randomly distributed SiO_x particles. Consequently, the SEI undergoes regeneration at the interface of the newly exposed active material, resulting from repeated physical fragmentation. This process ultimately manifests itself macroscopically as electrode-level expansion. Nevertheless, while the presence of SEI and interphase sequential lithiation facilitates lithium-ion transport, the irreversible microstructural damage ultimately hinders the complete lithiation process and the kinetics of the delithiation process. In view of the aforementioned, the mismatch between the physical properties of the graphite and SiO_x material represents a key factor in capacity degradation. Overcoming the stress dissipation and evolution is bound to the development of composite anode with higher reversible capacity and better electrochemical performance.

Acknowledgements

H.S. acknowledges the Macau Science and Technology Development Fund (FDCT) for funding FDCT no. 0013/2024/RIB1, FDCT-MOST joint project no. 0026/2022/AMJ, and grant no. 006/2022/ALC of the Macao Centre for Research and Development in Advanced Materials (2022–2024), the Shenzhen-Hong Kong-Macau Science and Technology Plan Project (Category C) (grant no. SGDX20220530111004028), the Multi-Year Research Grant (MYRG) from University of Macau (project nos. MYRG-GRG2023-00140-IAPME-UMDF and MYRG-GRG2024-00206-IAPME), Natural Science Foundation of Guangdong Province (grant no. 2023A1515010765), and Science and Technology Program of Guangdong Province of China (grant no. 2023A0505030001).

Conflict of Interest

The authors declare no conflict of interest.

Data Availability Statement

The data that support the findings of this study are available on request from the corresponding author. The data are not publicly available due to privacy or ethical restrictions.

Keywords: capacity fading mechanisms · composite anodes · lithium-ion batteries · SiO_x · solid electrolyte interfaces

[1] S. Weng, G. Yang, S. Zhang, X. Liu, X. Zhang, Z. Liu, M. Cao, M. N. Ateş, Y. Li, L. Chen, Z. Wang, X. Wang, *Nano-Micro Lett.* **2023**, *15*, 215.
[2] J. Lin, L. Wang, Q. Xie, Q. Luo, D. Peng, C. Buddie Mullins, A. Heller, *Angew. Chem., Int. Ed.* **2023**, *62*, e202216557.
[3] H. L. Andersen, L. Djuandhi, U. Mittal, N. Sharma, *Adv. Energy Mater.* **2021**, *11*, 2102693.
[4] Y. Yang, W. Yuan, W. Kang, Y. Ye, Q. Pan, X. Zhang, Y. Ke, C. Wang, Z. Qiu, Y. Tang, *Sustainable Energy Fuels* **2020**, *4*, 1577.
[5] D. J. Chung, D. Youn, J. Y. Kim, W. J. Jeong, S. Kim, D. Ma, T. R. Lee, S. T. Kim, H. Kim, *Small* **2022**, *18*, 2202209.
[6] S. Chae, S. H. Choi, N. Kim, J. Sung, J. Cho, *Angew. Chem., Int. Ed.* **2020**, *59*, 110.
[7] H. Tian, H. Tian, W. Yang, F. Zhang, W. Yang, Q. Zhang, Y. Wang, J. Liu, S. R. P. Silva, H. Liu, G. Wang, *Adv. Funct. Mater.* **2021**, *31*, 2101796.
[8] a) W. Wang, M. K. Datta, P. N. Kumta, *J. Mater. Chem.* **2007**, *17*, 3229; b) K. Kierzek, J. Machnikowski, F. Béguin, *J. Appl. Electrochem.* **2015**, *45*, 1; c) Q. Shi, J. Zhou, S. Ullah, X. Yang, K. Tokarska, B. Trzebicka, H. Q. Ta, M. H. Rümmeli, *Energy Storage Mater.* **2021**, *34*, 735.
[9] A. Guerfi, P. Charest, M. Dontigny, J. Trottier, M. Lagacé, P. Hovington, A. Vijh, K. Zaghib, *J. Power Sources* **2011**, *196*, 5667.
[10] D. H. S. Tan, Y. T. Chen, H. Yang, W. Bao, B. Sreenarayanan, J. M. Doux, W. Li, B. Lu, S. Y. Ham, B. Sayahpour, J. Scharf, E. A. Wu, G. Deysher, H. E. Han, H. J. Hah, H. Jeong, J. B. Lee, Z. Chen, Y. S. Meng, *Science* **2021**, *373*, 1494.
[11] J. Wu, Y. Cao, H. Zhao, J. Mao, Z. Guo, *Carbon Energy* **2019**, *1*, 57.
[12] a) K. P. C. Yao, J. S. Okasinski, K. Kalaga, J. D. Almer, D. P. Abraham, *Adv. Energy Mater.* **2019**, *9*, 1803380; b) S. B. Son, L. Cao, T. Yoon, A. Cresce, S. E. Hafner, J. Liu, M. Groner, K. Xu, C. Ban, *Adv. Sci.* **2019**, *6*, 1801007; c) X. Wang, J. Zhu, H. Dai, C. Yu, X. Wei, *Batteries* **2023**, *9*, 242.
[13] J. Moon, H. C. Lee, H. Jung, S. Wakita, S. Cho, J. Yoon, J. Lee, A. Ueda, B. Choi, S. Lee, K. Ito, Y. Kubo, A. C. Lim, J. G. Seo, J. Yoo, S. Lee, Y. Ham, W. Baek, Y. G. Ryu, I. T. Han, *Nat. Commun.* **2021**, *12*, 2714.
[14] W. M. Dose, M. J. Piernas-Muñoz, V. A. Maroni, S. E. Trask, I. Bloom, C. S. Johnson, *Chem. Commun.* **2018**, *54*, 3586.
[15] B. S. Lee, S. H. Oh, Y. J. Choi, M. J. Yi, S. H. Kim, S. Y. Kim, Y. E. Sung, S. Y. Shin, Y. Lee, S. H. Yu, *Nat. Commun.* **2023**, *14*, 150.
[16] Q. Sun, J. Li, M. Yang, S. Wang, G. Zeng, H. Liu, J. Cheng, D. Li, Y. Wei, P. Si, Y. Tian, L. Ci, *Small* **2023**, *19*, 2300759.
[17] P. Heugel, J. Petit, F. Klein, J. Tübke, *Batteries* **2023**, *9*, 449.
[18] T. Liu, L. Lin, X. Bi, L. Tian, K. Yang, J. Liu, M. Li, Z. Chen, J. Lu, K. Amine, K. Xu, F. Pan, *Nat. Nanotechnol.* **2019**, *14*, 50.
[19] M. Bin Jassar, C. Michel, S. Abada, T. De Bruin, S. Tant, C. Nieto-Draghi, S. N. Steinmann, *Adv. Funct. Mater.* **2024**, *34*, 2313188.

[20] S.-P. Kim, A. C. T. van Duin, V. B. Shenoy, *J. Power Sources* **2011**, *196*, 8590.
[21] S. Y. Sun, N. Yao, C. Bin Jin, J. Xie, X. Y. Li, M. Y. Zhou, X. Chen, B. Q. Li, X. Q. Zhang, Q. Zhang, *Angew. Chem., Int. Ed.* **2022**, *61*, e202208743.
[22] S. T. Oyakhire, H. Gong, Y. Cui, Z. Bao, S. F. Bent, *ACS Energy Lett.* **2022**, *7*, 2540.
[23] J. Park, S. S. Park, Y. S. Won, *Electrochim. Acta* **2013**, *107*, 467.
[24] Q. Sun, G. Zeng, J. Li, S. Wang, M. Botifoll, H. Wang, D. Li, F. Ji, J. Cheng, H. Shao, Y. Tian, J. Arbiol, A. Cabot, L. Ci, *Small* **2023**, *19*, 2302644.

Manuscript received: February 20, 2025
Revised manuscript received: April 2, 2025
Version of record online: April 15, 2025